Journal of Theoretical and Applied Physics (2019) 13:155–164
https://doi.org/10.1007/s40094-019-0331-6

RESEARCH

Optical, magnetic characterization, and gamma-ray interactions for borate glasses using XCOM program

Y. S. Rammah[1] · A. S. Abouhaswa[1] · A. H. Salama[2] · R. El-Mallawany[1]

Received: 30 March 2019 / Accepted: 4 May 2019 / Published online: 15 May 2019

Abstract

In the present study, the optical characterization of borate glasses with composition $35Li_2O-10ZnO-55B_2O_3-xMnO_2$: $x=0$, 0.5, 1.0, 1.5, and 2.0 wt% has been investigated. The absorption spectra measurements within the wavelength domain 200–1000 nm have been carried out. The optical energy gap of the investigated samples using the absorption spectrum fitting (ASF) model has been calculated. The molar refraction, molar polarizability, reflection loss, optical transmission for the samples were estimated. The metallization criterion, dielectric constant, refractive index, and energy band metallization criterion for the studied glasses were estimated. Magnetic property measurements for all glass samples were carried out at 300 K. Additionally, the prospects of gamma-ray interactions with the investigated glasses have been achieved through studying the total mass attenuation, coherent, Compton, photoelectric, and pair production interactions at photon energy in the range of 0.356–1.330 MeV. Results reveal that the optical and magnetic properties of the investigated glasses change with changing the MnO_2 concentration. Studied glasses can be used as a candidate for optical fiber and optical devices application. In the other hand, at lower gamma photon energy range, the photoelectric absorption dominates with the glasses, while as the energy increases, the probability of Compton scattering and pair production become the most dominate interactions.

Keywords Borate glasses · Molar refraction · Molar polarizability · Attenuation · Gamma interaction

Introduction

Currently, in medical, industrial, and academic applications, glasses containing transition metal oxides have great interest and more attractive [1–8]. Most of the previous studies confirm that the optical characterization of this type of glasses may be changed with addition of different transition metal oxides with different concentrations. Oxide glasses have growing importance due to their application in low-loss optical fibers, as the dispersion properties changed with the composition. In the other hand, dispersion measurements are important in the designing of high bandwidth infrared optical fibers and optical communication devices [9]. It is known that boron (B), phosphorous (P), and silicon (Si) oxides considered as the typical glass forming oxides, and they have high potential for technological applications. Borate glasses considered as one of the most attractive, brilliant, and preferred host glass former materials. It is a prime constituent of numerous large volume industrial glasses [10–13]. This is because, when alkali oxides add to the covalent boron oxide amorphous system, a significant change will be occurred, resulting in the creation of anionic sites that accommodate the modifying alkali cations [14, 15].

Previously, borate glass doped with MnO_2 has been prepared [1]. FTIR, XRD, and the optical properties including the optical energy gap, Urbach's energy, refractive index, optical conductivity for these glasses have been studied [1].

The main objective of the current work is to:

1. Investigate the optical characterization of borate glasses with composition $35Li_2O-10ZnO-55B_2O_3-xMnO_2$: $x=0$, 0.5, 1.0, 1.5, and 2.0 wt% and this achieved by;
    i. Measuring the absorption spectra within the wavelength domain 200–1000 nm.

✉ Y. S. Rammah
dr_yasser1974@yahoo.com

[1] Department of Physics, Faculty of Science, Menoufia University, Shebin El-Koom 32511, Egypt

[2] Department of Physical Chemistry, Inorganic Chemical Industries and Mineral Resources Division, National Research Centre, 33 El Bohouth St.- Dokki, Giza, Egypt

ii. Estimating the optical energy gap of the investigated samples using the absorption spectrum fitting (ASF) model.
iii. Calculating the molar refraction, molar polarizability, reflection loss, and optical transmission for the samples.
iv. Estimating the metallization criterion, dielectric constant, refractive index, and energy band metallization criterion for the studied glasses.

2. Study the magnetic property of the studied glasses.
3. Investigate the prospects of gamma-ray interactions with the investigated glasses and this achieved through studying the total mass attenuation, coherent, Compton, photoelectric, and pair production interactions.

Samples and calculations

The investigated glass samples in this study were prepared before and adapted from [1]. The density (ρ) of glasses was measured by Archimedes' principle using a digital balance and toluene with density 0.86 gm/cm^3 as an immersion liquid at room temperature. The accuracy of the measurements was approximately ± 0.01 gm/cm^3. Molar volume (V_m) of each glass has been calculated by using its density and molecular weight. Densities and molar volumes for present glasses are listed in Table 1. In this study, the optical measurements which are obtained by JASCO UV–Vis–NIR double-beam spectrophotometer model V-570 in the range of 200–1000 nm wavelength are used to investigate many of important optical characterization of the glass samples. Magnetic property measurements for all glass samples were carried out at 300 K with a vibrating sample magnetometer (VSM 7400 Lakeshore, Max field = 20 kOe, USA).

Mass attenuation coefficient and probability of γ-interaction

In nuclear shielding, the fundamental physical quantity is the mass attenuation coefficient (μ/ρ) which used to produce the other photon interaction parameters such as effective atomic number, half value layer. For any material, μ/ρ can be evaluated by the mixture rule given by [16]:

$$\mu/\rho = \sum_i w_i(\mu/\rho)_i \tag{1}$$

where w_i is the weight fraction of element i and $(\mu/\rho)_i$ is the mass attenuation coefficient of the ith element. In this study, the μ/ρ for the studied glasses was determined by the XCOM program [17].

According to knowledge of nuclear physics, gamma photon interacts with the medium by three main processes, namely photoelectric effect (τ), Compton scattering (σ), and pair production (κ). The total linear attenuation coefficient (μ) which expressed to the total probability of the interaction is equal to the sum of the partial probabilities of the different processes [18]:

$$\mu = \tau + \sigma + \kappa \tag{2}$$

The probability of occurrence for these interaction processes can be derived from the following g relations:

$$\left.\begin{aligned} \tau(\mathrm{cm}^{-1}) &= cN\left(\frac{Z^b}{E_\gamma^a}\right)\left[1 - f(Z)\right], \\ \sigma(\mathrm{cm}^{-1}) &= NZf(E_\gamma), \\ \kappa(\mathrm{cm}^{-1}) &= NZ^2 f(E_\lambda, Z) \end{aligned}\right\} \tag{3}$$

where c is a constant coefficient, independent of Z and E_γ. Parameters a and b are constants with values between 3 and 5 depending on gamma energy. N is atomic density, and Z is atomic number. The probabilities of γ-ray interaction with the studied glasses have been calculated theoretically using XCOM program [17].

Table 1 Density (ρ), molar volume (V_m), optical energy band gap ($E_{Opt.}^{Tauc}$ and $E_{Opt.}^{ASF}$ eV), and refractive index (n) via Tacu's and ASF methods for glass samples in the system $(35Li_2O - 10ZnO - 55B_2O_3) + xMnO_2$: $0 \le x \le 2$ wt%) glasses

$xMnO_2$ (wt%) x =	Density (ρ) (± 0.01 g/cm^3)	Molar volume (V_m) (cm^3/mol)	$E_{Opt.}^{Tauc}$ (eV) via Tauc's method [1]		$E_{Opt.}^{ASF}$ (eV) via ASF method [present work]		Refractive index, n	
			Indirect	Direct	Indirect	Direct	Tauc's method	ASF method
0.0	2.9412	19.3725	2.91	3.25	2.85	3.23	2.4217	2.4386
0.5	2.9367	19.51861	3.13	3.31	3.1	3.34	2.3629	2.3706
1.0	2.9319	19.6984	2.93	3.28	2.97	3.28	2.4161	2.4052
1.5	2.9287	19.6984	2.90	3.26	2.95	3.24	2.4245	2.4106
2.0	2.9257	20.0372	3.07	3.29	3.04	3.31	2.3784	2.3863

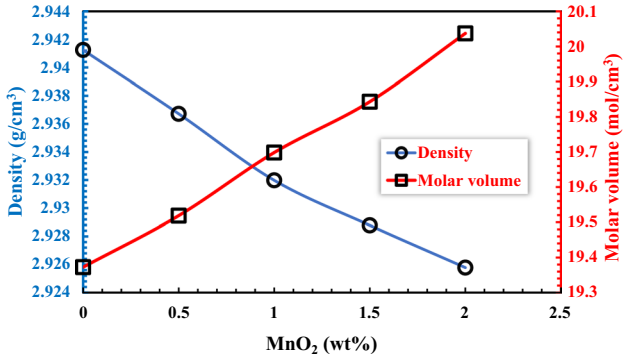

Fig. 1 Variation of density and molar volume of $35Li_2O-10ZnO-55B_2O_3-xMnO_2$: $x=0$, 0.5, 1.0, 1.5, and 2.0 wt% glass system with MnO_2 concentration

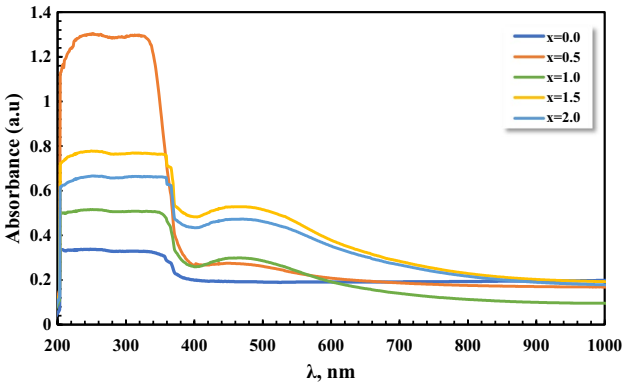

Fig. 2 UV-visible spectra of the studied glass system

Results and discussion

Density and molar volume

Figure 1 depicts the variation of density (ρ) and molar volume (V_m) with different MnO_2 concentrations in the glasses. The decrease in the glass density is most likely due to lower atomic mass of Mn ions as compared to Zn in glass system. Therefore, decreased oxygen packing density makes the structure more compact and this result decreasing of the bridging oxygen number [19]. Also, Fig. 1 shows that molar volume of the samples has an exactly opposite behavior to that of density. The rate of change in molar volume mainly depends on the rates of change of both molecular weight and density. With increasing MnO_2 concentration, the molecular weights decrease due to addition of some lighter Mn^{+2} ions and the density decreases and this is accompanied by increase in molar volume.

Optical characterization

UV–visible spectra

Figure 2 demonstrates the measured optical absorption spectra for the investigated glasses. It is clear to notice that the broad absorption band around 475 nm, which is assigned to the transition $^6A_{1g}(S)\rightarrow{}^4T_{1g}$ (G) of Mn^{2+}ions [20]. In addition, the absorbance of this absorption band enhanced with increasing MnO_2 concentration in the glass samples which could be due to relatively large average distance between Mn^{2+} ions [21].

The optical energy gap $\left(E_{Opt.}^{ASF}\right)$ and refractive index (n)

In the present work, the absorption spectrum fitting (ASF) model [22, 23] has been applied to calculate the optical energy band gaps $E_{Opt.}^{ASF}$ for the investigated glasses using the measured UV-absorption spectra. This method is characterized by the calculation of the optical gap energy of the samples can be achieved without need to thickness measurement. The calculation mainly only depends on an absorbance data of the samples. Mott and Davis [24] have modified Tauc's formula [25] for the optical absorption coefficient $\alpha(\omega)$ to be written as:

$$\alpha(\omega)\hbar\omega = K\left(\hbar\omega - E_{Opt.}^{ASF}\right)^m \tag{4}$$

Beer–Lambert's law is used to calculate $\alpha(\omega)$. G, $\hbar\omega$, and $E_{Opt.}^{ASF}$ are a constant, the incident photon energy, and the band gap energy. The optical transition type can be characterized by the power (m), where $m=0.5$ and 2, respectively, for allowed direct and indirect transitions [26]. Alarcon et al. [22], Souri and Shomalian [23] have expressed for the optical gap energy $\left(E_{Opt.}^{ASF}\right)$ as a function of incident photon wavelength $\lambda_{Opt.}^{ASF}$ as:

$$E_{Opt.}^{ASF} = \frac{hc}{\lambda_{Opt.}^{ASF}} = \frac{1239.83}{\lambda_{Opt.}^{ASF}} \tag{5}$$

Figures 3 and 4 illustrate the variation of (absorbance/wavelength)$^{1/2}$ and (absorbance/wavelength)^2 with (wavelength)$^{-1}$ for indirect and direct transitions, respectively. The obtained values of $E_{Opt.}^{ASF}$ are calculated and listed in Table 1. These values are close to which obtained by using Tauc's model in the previous work [1]. Results reveal that the $E_{Opt.}^{ASF}$ for direct and indirect transitions for the samples changed with the variation of MnO_2 wt%. This variation in optical band gap after adding the Mn to the glass matrix is because of the Mn defects within the bands [27]. These Mn^{2+} defects will result in the absorption of incident photons. Therefore, the band gap is affected due to the strong internal forces. The electrons

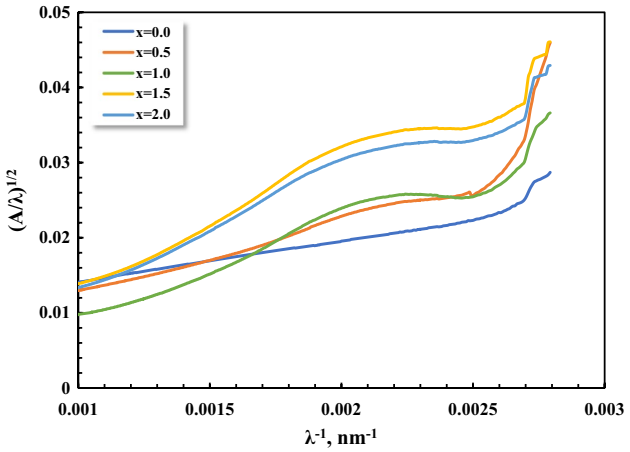

Fig. 3 Variation of $(A/\lambda)^{1/2}$ with λ^{-1} for all investigated glasses

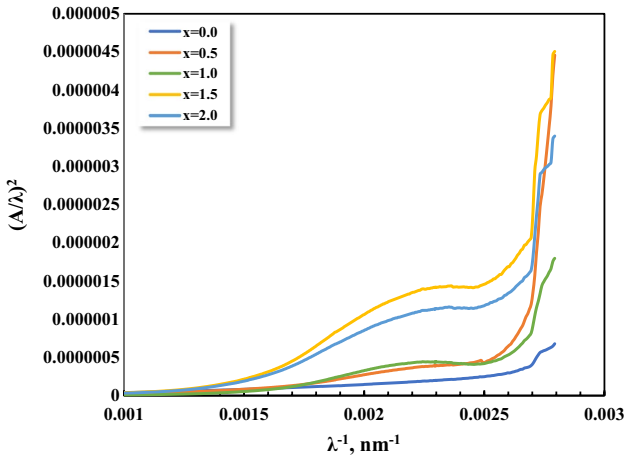

Fig. 4 Variation of $(A/\lambda)^2$ with λ^{-1} for all investigated glasses

are liable for the transition between the valence and conduction bands but need greater energy to leap [1]. Figure 5 shows a comparison between $E_{\text{Opt.}}^{\text{ASF}}$ values for direct and indirect cases, one obvious that the values for direct case are higher than that for indirect case.

Using the obtained values of the optical energy gap $E_{\text{Opt.}}^{\text{ASF}}$, refractive index ($n$) of the glass system was calculated by the following equation [28, 29] and collected in Table 1:

$$\left(\frac{n^2-1}{n^2+2}\right) = 1 - \sqrt{\frac{E_{\text{Opt.}}^{\text{AsF}}}{20}} \tag{6}$$

Results revealed that the refractive index of all glasses is high, and they become more interesting and potential candidates for optical filter materials and optoelectrical devices.

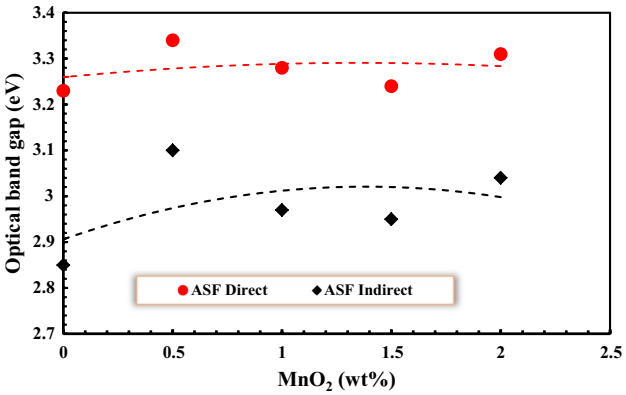

Fig. 5 Variation of optical energy gap with MnO_2 concentration in ASF and Tauc's models

(R_m), (α_m), (R_L), and (T)

The degree of the total polarizability per unit mole is defined as the molar refraction (R_m) of material. The (R_m) relates to molar volume (V_m) and index of refraction (n) via Lorentz-Lorenz equation [30, 31]:

$$R_m = \left(\frac{n^2-1}{n^2+2}\right)\frac{M_{\text{glass}}}{\rho_{\text{glass}}} = \left(\frac{n^2-1}{n^2+2}\right)V_m \tag{7}$$

where ρ_{glass} and M_{glass} are the density of the glass sample and the molar mass, respectively. The (R_m) for the glasses was calculated using Eq. (7) and listed in Table 2. The electronic polarizability (α_m) of a molecule gives the magnitude of electrons responding to an electric field can be expressed as a function of molar refraction as in Eq. (8) [32, 33]:

$$\alpha_m = \frac{R_m}{2.52} \tag{8}$$

The values of (α_m) are calculated and listed Table 2. Figure 6 plots the relation between (R_m) and (α_m) as a function of MnO_2 concentration in the studied glass system. It is clear that (R_m) and (α_m) have the same behavior for the investigated glass samples.

Reflection loss (R_L), and optical transmission (T)

The reflection loss (R_L) and optical transmission (T) for the studied glasses were estimated by using Eqs. (9) and (10), respectively, and tabulated in Table 2.

$$R_L = \left(\frac{n-1}{n+1}\right)^2 \tag{9}$$

$$T = \frac{2n}{n^2+1} \tag{10}$$

Table 2 Molar refraction (R_m), electronic polarizability (α_m), reflection loss (R_L), optical transmission (T) for glass samples in the system $(35Li_2O-10ZnO-55B_2O_3)+xMnO_2$: $0 \le x \le 2$ wt%) glasses

$xMnO_2$ (wt%) x =	Molar refraction (R_m)	Electronic polarizability ($\alpha_m \times 10^{-24}$ cm^3)	Reflection loss (R_L)	Optical transmission (T)	Metallization criterion (M)	Dielectric constant (ε)	Refractive index-based metallization criterion M (n)	Energy gap-based metallization criterion $M\left(E_g^{ASF}\right)$
0.0	13.7954	5.4743	0.1750	0.7020	0.2878	5.9471	0.3774	0.3774
0.5	13.6217	5.4054	0.1653	0.7162	0.3021	5.6200	0.3937	0.3937
1.0	13.8919	5.5126	0.1702	0.7089	0.2947	5.7849	0.3853	0.3853
1.5	14.0166	5.5621	0.1710	0.7078	0.2936	5.8113	0.3840	0.3840
2.0	14.0513	5.5759	0.1676	0.7129	0.2987	5.6948	0.3898	0.3898

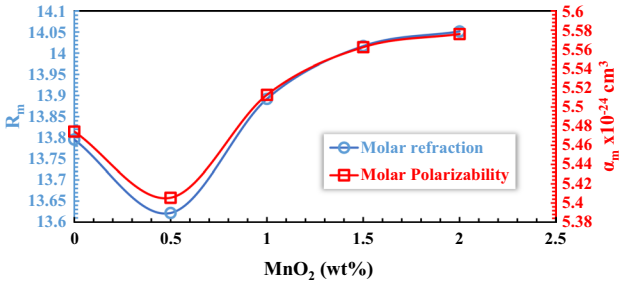

Fig. 6 Variation of R_m and α_m for all glasses with MnO_2 concentration

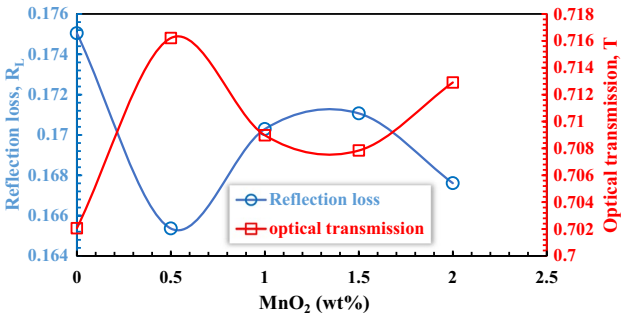

Fig. 7 Variation of R_L and T for all glasses with MnO_2 concentration

The variation of these parameters versus MnO_2 concentration is depicted in Fig. 7. Results confirm that R_L and T have an opposite behavior with MnO_2 content.

(*M*), (ε), *M* (*n*), and M $\left(E_{Opt.}^{ASF}\right)$

In order to estimate the tendency of metallization and to investigate the insulating behavior of the studied glasses, metallization criterion (M) is calculated theoretically according to the metallization theory for condensed matter as Herzfeld [34]. In this theory, predicting of the metallic nature or otherwise of solids depends on the necessary and sufficient condition which is $\frac{R_m}{V_m} > 1$ for metallic nature and $\frac{R_m}{V_m} < 1$ for non-metallic nature [35, 36]. The values of (M) for the studied glasses were obtained by subtracting the ratio (R_m/V_m) by 1 [37].

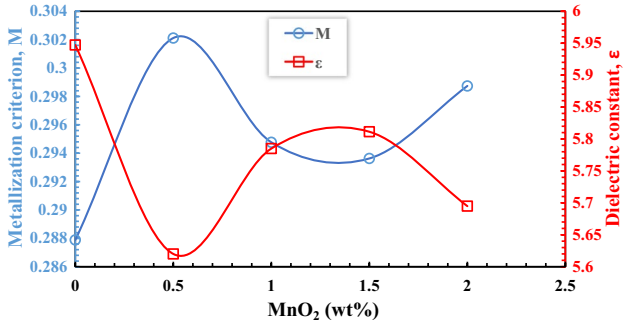

Fig. 8 Variation of M and ε for all glasses with MnO_2 concentration

The dielectric constant (ε) for the present glasses was calculated by $\varepsilon = n^2$[38]. The values of (M) and (ε) are calculated, tabulated in Table 2 and depicted versus the MnO_2 concentration as shown in Fig. 8. Results reveal that the behavior of metallization criterion and dielectric constant for the present glass system is inversely with MnO_2 content.

M (n) and $M\left(E_{Opt.}^{ASF}\right)$ are the metallization criterions based on index refraction and optical energy band gap, respectively. These two optical properties have been calculated using [37]:

$$M(n) = 1 - \left(\frac{n^2 - 1}{n^2 + 2}\right) \tag{11}$$

$$M(E_{Opt.}^{ASF}) = \left(\frac{E_{Opt.}^{ASF}}{20}\right)^{1/2} \tag{12}$$

The values of M (n) and $M\left(E_{Opt.}^{ASF}\right)$ for the present system were calculated, listed in Table 2, and plotted versus MnO_2 concentration in Fig. 9. Figure 9 shows that both the M (n) and the $M\left(E_{Opt.}^{ASF}\right)$ have the same trend, enhancing with the increasing MnO_2 content. This indicates a decreasing chance

of metallization in the electronic structure of the studied glass system with increasing MnO_2 content.

Magnetic property of the studied glasses

Figure 10 displays the magnetization (M) as a function of magnetic field (H) of $35Li_2O-10ZnO-55B_2O_3+xMnO_2$ (where $x=0$, 0.5, 1.5, 2, and 2.5 wt%) glass samples

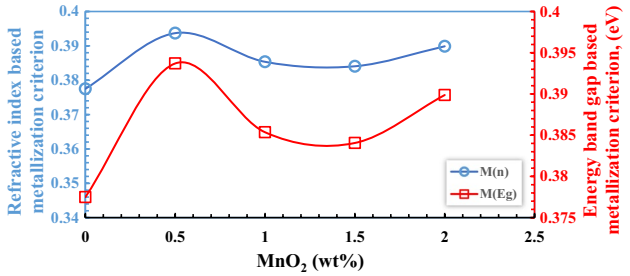

Fig. 9 Variation of M (n) and $M\left(E_{\text{Opt.}}^{\text{ASF}}\right)$ in (eV) for all glasses with MnO_2 concentration

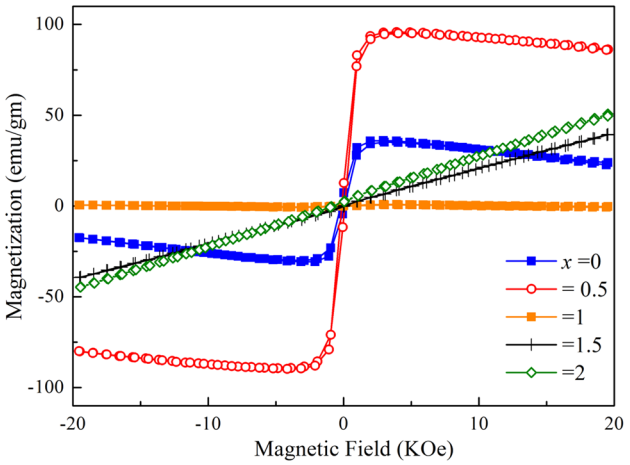

Fig. 10 Magnetization versus applied magnetic field of $35Li_2O-10ZnO-55B_2O_3+xMnO_2$ ($x=0$, 0.5, 1, 1.5, and 2) glass samples at 300 K

measured by a vibrating sample magnetometer (VSM) at room temperature. It was observed that undoped glass exhibited a soft ferromagnetic behavior; the hysteretic loop indicated a ferromagnetic behavior with magnetic coercivity about (180.35 Oe) and saturation magnetization M_s about (23.9 emu/gm). At the beginning of doping, the sample with $x=0.5$ wt% showed the highest saturation magnetization (86.25 emu/g) and magnetic coercivity (183.32 Oe). However, the glass samples doped with MnO_2 at 1-2 wt% showed a paramagnetic behavior and the magnetization decreased with increasing MnO_2 content. The mechanism for the highest saturation magnetization M_s at $x=0.5$ may be related with the exchange coupling between anti-ferromagnetic phase and ferromagnetic-like phase as that in BaO [39, 40]. On the other hand, decreasing of saturation magnetization M_s with increasing doping concentration might be due to the increasing anti-ferromagnetic phase with small ratio of ferromagnetic-like phase [41–43]. It is fascinating to note when the doping concentration is higher than 1 wt% a linear M–H curve is observed, and the magnetization is much smaller than undoped sample. This suggests that the sample may become anti-ferromagnetic again. This provides one of the main uses in so-called spin valves, which are the basis of magnetic sensors including modern hard drive read heads.

Probabilities of γ-ray interaction

Table 3 shows the chemical composition and weight fraction of elements in the studied glass samples. The total mass attenuation coefficients (μ/ρ) and the partial interaction between gamma-ray with different energies (0.356, 0.511, 0.662, 1.173, and 1.330 MeV) and the suggested glass system were computed using Eqs. (1) and (3), respectively, via XCOM program. The μ/ρ for the studied glasses reduced with the increase in the photon energy from 0.356 to 1.330 MeV approximately by the same rate at all MnO_2 concentrations as shown in Table 4 and Fig. 11. The XCOM obtained values of the μ/ρ were compared with available experimental data which measured using narrow beam transmission geometry (see Table 4 and Fig. 11). Figure 12 shows a comparison between experimental and XCOM

Table 3 Chemical composition and Wt. fraction of elements in samples in the system $(35Li_2O-10ZnO-55B_2O_3)+xMnO_2$: $0\le x\le 2$ wt%) glasses

$xMnO_2$ (wt%) x =	Sample chemical composition	Weight fraction wt%				Wt. fraction of elements in each sample				
		Li_2O	ZnO	B_2O_3	MnO_2	Li	B	O	Zn	Mn
0.0	$35Li_2O-10ZnO-55B_2O_3+0.0MnO_2$ wt%	35	10	55	0.0	0.162599	0.170814	0.586244	0.080342	0.000000
0.5	$35Li_2O-10ZnO-55B_2O_3+0.5MnO_2$ wt%	35	10	55	0.5	0.161791	0.169964	0.585159	0.079942	0.003144
1.0	$35Li_2O-10ZnO-55B_2O_3+1.0MnO_2$ wt%	35	10	55	1.0	0.160990	0.169123	0.584084	0.079547	0.006257
1.5	$35Li_2O-10ZnO-55B_2O_3+1.5MnO_2$ wt%	35	10	55	1.5	0.160197	0.168290	0.583020	0.079155	0.009339
2.0	$35Li_2O-10ZnO-55B_2O_3+2.0MnO_2$ wt%	35	10	55	2.0	0.159411	0.167465	0.581966	0.078767	0.012391

Table 4 Total mass attenuation coefficients (μ_m) of $(35Li_2O-10ZnO-55B_2O_3)+xMnO_2$: $0\le x\le 2$ wt%) glasses

Energy (MeV)	$x=0$ $\mu_m\times10^{-2}$ (cm^2/g)		$x=0.5$ $\mu_m\times10^{-2}$ (cm^2/g)		$x=1$ $\mu_m\times10^{-2}$ (cm^2/g)		$x=1.5$ $\mu_m\times10^{-2}$ (cm^2/g)		$x=2$ $\mu_m\times10^{-2}$ (cm^2/g)	
	XCOM	Exp.	XCOM	Exp.	XCOM	Exp.	XCOM	Exp.	XCOM	Exp.
0.356	9.60	9.62	9.60	9.64	9.60	9.63	9.60	9.64	9.61	9.65
0.511	8.28	8.31	8.29	8.33	8.29	8.33	8.29	8.33	8.29	8.34
0.662	7.40	7.42	7.40	7.44	7.74	7.45	7.40	7.45	7.40	7.44
1.173	5.63	5.66	5.64	5.69	5.64	5.67	5.64	5.68	5.64	5.68
1.330	5.28	5.32	5.29	5.34	5.29	5.34	5.29	5.34	5.29	5.34

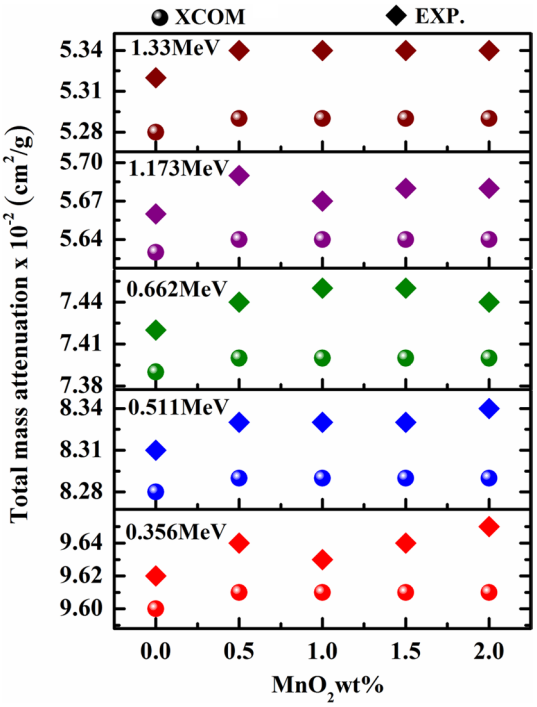

Fig. 11 Dependence of the μ/ρ for all glasses on MnO_2 concentration (experimentally and XCOM program)

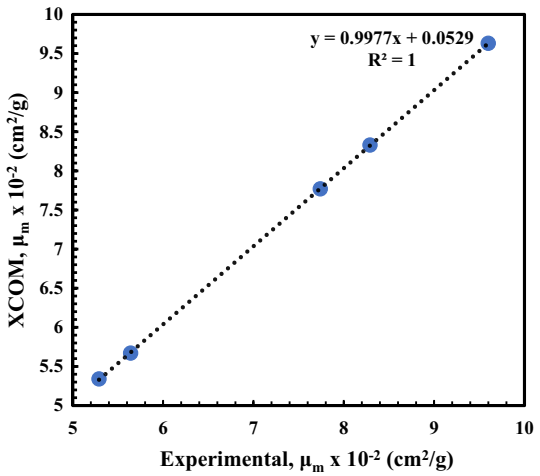

Fig. 12 Comparison between experimental and XCOM (μ_m) for glass sample with $MnO_2=1$ wt%

(μ_m) for glass sample with $MnO_2=1$ wt%. R^2 values which define the degree of agreement between the theoretical and experimental data were evaluated; results are found to be 0.9977 (i.e., ~ 1) for all studied samples and therefore prove that the results are in a well agreement. This result implies that: (i) The gamma radiation attenuation rate do not change with addition of MnO_2 in the studied glasses, (ii) At the lower energy, the gamma photon has higher probability of interaction with the studied glasses. Also, it is obvious that when the photon energy increases from 0.356 to 0.662 MeV ($E<0.662$ MeV), the total mass attenuation coefficients (μ/ρ) reduced very quickly by high rate, while in the range of ($E>0.662$ MeV), the μ/ρ reduced by low rate. For example, in the glass sample ($xMnO_2=1$ wt%), the difference in the μ/ρ between 0.356 and 0.511 MeV is $1.31x10^{-2}$ (cm^2/g), while the difference in the μ/ρ between 1.173 and 1.330 MeV is $0.35x10^{-2}$ (cm^2/g). This behavior in the total mass attenuation coefficients (μ/ρ) can be explained as follows: at lower gamma photon energy range, the photoelectric absorption dominates, and this is confirmed by data in Table 5. While as the energy increases, the probability of the photoelectric absorption process is reduced and other two processes namely Compton scattering (Table 6) and pair production (P.P) (Table 7 and Fig. 13) become the most dominate interactions, where this occurs specifically for $E>1.022$ MeV [44, 45]. These results (dependent of μ/ρ on the photon energy) are corresponding with the recently published literature on different materials like rocks [44], glasses [46–50], bricks [51], and amino acids [52]. Comparison with other glasses; like tellurite glasses [53–55] could be suggested.

Table 5 Photoelectric interaction of $(35Li_2O-10ZnO-55B_2O_3)+xMnO_2$: $0\le x\le 2$ wt%) glasses

Energy (MeV)	$x=0$ Photoelectric interaction ($\times 10^{-4}$ cm^2/g)	$x=0.5$ Photoelectric interaction ($\times 10^{-4}$ cm^2/g)	$x=1$ Photoelectric interaction ($\times 10^{-4}$ cm^2/g)	$x=1.5$ Photoelectric interaction ($\times 10^{-4}$ cm^2/g)	$x=2$ Photoelectric interaction ($\times 10^{-4}$ cm^2/g)
0.356	6.22	6.31	6.40	6.48	6.57
0.511	2.34	2.37	2.41	2.44	2.47
0.662	1.22	1.24	1.26	1.28	1.30
1.173	0.36	0.36	0.36	0.37	0.38
1.330	0.28	0.29	0.29	0.30	0.30

Table 6 Compton interaction of $(35Li_2O-10ZnO-55B_2O_3)+xMnO_2$: $0\le x\le 2$ wt%) glasses

Energy (MeV)	x=0 Compton interaction ($\times 10^{-2}$ cm^2/g)	x=0.5 Compton interaction ($\times 10^{-2}$ cm^2/g)	x=1 Compton interaction ($\times 10^{-2}$ cm^2/g)	x=1.5 Compton interaction ($\times 10^{-2}$ cm^2/g)	x=2 Compton interaction ($\times 10^{-2}$ cm^2/g)
0.356	9.54	9.54	9.54	9.54	9.54
0.511	8.29	8.26	8.26	8.26	8.26
0.662	7.39	7.38	7.39	7.39	7.39
1.173	5.63	5.63	5.63	5.63	5.63
1.330	5.28	5.28	5.30	5.28	5.28

Table 7 Pair production (P.P) interaction of $(35Li_2O-10ZnO-55B_2O_3)+xMnO_2$: $0\le x\le 2$ wt%) glasses

Energy (MeV)	$x=0$ P.P interaction ($\times 10^{-5}$ cm^2/g)	$x=0.5$ P.P interaction ($\times 10^{-5}$ cm^2/g)	$x=1$ P.P interaction ($\times 10^{-5}$ cm^2/g)	$x=1.5$ P.P interaction ($\times 10^{-5}$ cm^2/g)	$x=2$ P.P interaction ($\times 10^{-5}$ cm^2/g)
1.173	0.74	0.75	0.76	0.76	0.77
1.330	4.29	4.32	4.35	4.38	4.40

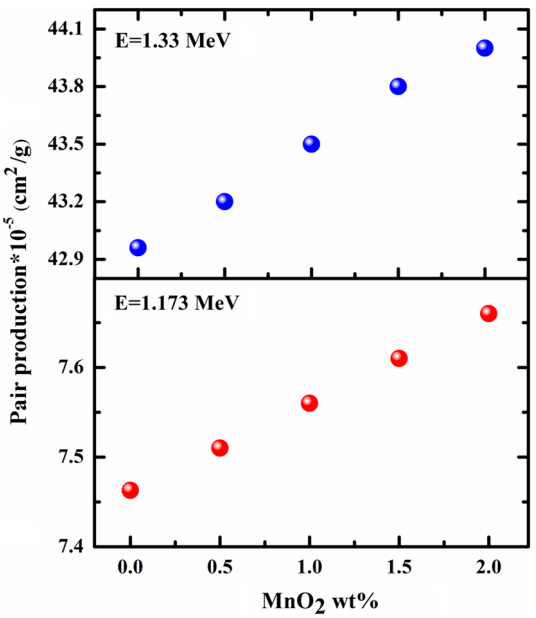

Fig. 13 Dependence of the (P.P) interaction for all glasses on MnO_2 concentration

Conclusion

In the present study, the optical characterization of borate glasses with composition $35Li_2O-10ZnO-55B_2O_3-xMnO_2$: $x=0$, 0.5, 1.0, 1.5, and 2.0 wt% which prepared previously [1] has been investigated. The absorption spectra measurements within the wavelength domain 200–1000 nm have been carried out. The optical energy gap of the investigated samples using the absorption spectrum fitting (ASF) model has been calculated. The probabilities of gamma-ray interactions with the investigated glasses have been achieved through studying the total mass attenuation using XCOM program. In general, the results reveal the following items:

1. The optical energy gap of the studied glasses varies with $xMnO_2$ content in both of direct and of indirect transitions.

2. The molar refraction and molar polarizability for the investigated glasses have the same trend with MnO_2 content.
3. The reflection loss and optical transmission for the samples have an opposite behavior with MnO_2 concentration.
4. The behavior of metallization criterion and dielectric constant for the present glass system is inversely with MnO_2 content.
5. Refractive index and energy band metallization criterion have the same trend, enhancing with the increasing MnO_2 content for the studied glasses.
6. Magnetic property of the investigated glasses changes with changing the MnO_2 concentration.
7. The μ/ρ for the studied glasses was reduced with the increase in the photon energy from 0.356 to 1.330 MeV; this confirms that at lower gamma photon energy range, the photoelectric absorption dominates, while at higher photon energy, Compton scattering and pair production become the most dominate interactions.

Results reveal that the investigated glasses can be used as a candidate for optical fiber and optical devices application. Moreover, it can be used for optoelectronic and nonlinear optical devices.

References

1. Taha, T.A., Abouhaswa, A.S.: Preparation and optical properties of borate glass doped with MnO_2. J. Mater. Sci. **29**, 8100–8106 (2018)
2. Taha, T.A., Rammah, Y.S.: Optical characterization of new borate glass doped with titanium oxide. J. Mater. Sci. **27**(2), 1384–1390 (2016)
3. Taha, T.A., Azab, A.A.: AC conductivity and dielectric properties of borotellurite glass. J. Electron. Mater. **45**(10), 5170–5177 (2016)
4. Yadav, A., Dahiya, M.S., Narwal, P., Hooda, A., Agarwal, A., Khasa, S.: Electrical characterization of lithium bismuth borate glasses containing cobalt/vanadium ions. Solid State Ion. **312**, 21–31 (2017)
5. Colak, S.C.: Role of titanium ions on the optical and thermal properties of zinc borate glass doped with TiO_2 physics and chemistry of glasses-European. J. Glass Sci. Technol. Part B **58**(2), 41–48 (2017)
6. Asahara, Y.: Non-linear glass materials. Ceram. Int. **23**(5), 375–382 (1997)
7. Yamada, S., Chen, W.D., Koeppen, C., Jiang, G., Shi, R.F., Garito, A.F.: Non-linear optical properties of organic materials VIII. SPIE **2527**, 2 (1995)
8. Abdel-Baki, M., Abdel-Wahab, F.A., Radi, A., El-Diasty, F.: Factors affecting optical dispersion in borate glass systems. J. Phys. Chem. Solids **68**(8), 1457–1470 (2007)
9. Saddeek, Y.B., Shaaban, E.R., Moustafa, H.M.: Spectroscopic properties, electronic polarizability, and optical basicity of Bi 2 O 3 –Li 2 O-B 2 O 3 glasses. Phys. B **403**(13–16), 2399–2407 (2008)
10. Varshneya, A.K.: Fundamentals of Inorganic Glasses. Academic Press, London (1994)
11. Kreidl, N.J.: Recent applications of glass science. J. Non-Cryst. Solids **123**(1–3), 377–384 (1990)
12. Vienna, J.: Nuclear waste glasses. In: Seward, T.P., Vascott, T. (eds.) High Temperature Glass Melt Property Database for Process Modeling, Properties of glass forming melts, pp. 391–404. Washington, DC, American Ceramic Society (2005)
13. El-Mallawany, R.: Structural interpretations on tellurite glasses. Mater. Chem. Phys. **63**(2), 109–115 (2000)
14. Chryssikos, G.D., Kamitsos, E.I., Karakassides, M.A.: Structure of borate glasses. Part 2. Alkali induced network modifications in terms of structure and properties. Phys. Chem. Glasses **31**(3), 109–116 (1990)
15. Saddeek, Y.B., Aly, K.A., Bashier, S.A.: Optical study of lead boro-silicate glasses. Phys. B **405**(10), 2407–2412 (2010)
16. Yılmaz, D., Boydaş, E., Cömert, E.: Determination of mass attenuation coefficients and effective atomic numbers for compounds of the 3d transition elements. Radiat. Phys. Chem. **125**, 65–68 (2016)
17. Berger, M.J., Coursey, J.S., Zucker, M.A., Chang, J.: ESTAR, PSTAR, and ASTAR: Computer Programs for Calculating Stopping-power and Range Tables for Electrons, Protons, and Helium Ions (Version 1.2.3), National Institute of Standards and Technology, Gaithersburg, MD (2005). http://physics.nist.gov/Star. Accessed 28 Sept 2006
18. Jalali, M., Mohammadi, A.: Gamma ray attenuation coefficient measurement for neutron-absorbent materials. Radiat. Phys. Chem. **77**, 523–527 (2008)
19. El-Rabaie, S., Taha, T.A., Higazy, A.A.: Compositional dependence thermal and optical properties of a novel germanate glass. Phys. B **432**, 40–44 (2014)
20. Raja, B.J., Yadav, M.R., Manjari, V.P., Babu, B., Krishna, C.R., Ravikumar, R.V.S.S.N.: Synthesis and characterization of undoped and Mn(II) ions doped Li_2 $CaAl_4(PO_4)_4F_4$ nanophosphors. J. Mol. Struct. **1076**, 461–467 (2014)
21. Samsudin, N.F., Matori, K.A., Liew, J.Y.C., Fen, Y.W., Zaid, M., Hafiz, M., Alassan, Z.N.: Investigation on structural and optical properties of Willemite doped Mn_2. J. Spectrosc **2015**, 7 (2015)
22. Alarcon, L.E., Arrieta, A., Camps, E., Muhl, S., Rudil, S., Santiago, E.V.: An alternative procedure for the determination of the optical band gap and thickness of amorphous carbon nitride thin films. Appl. Surf. Sci. **254**, 412–415 (2007)
23. Souri, D., Shomalian, K.: Band gap determination by absorption spectrum fitting method (ASF) and structural properties of different compositions of (60-x) V_2O_5-40TeO_2-xSb_2O_3 glasses. J. Non-Cryst. Solids **355**, 1597–1601 (2009)
24. Mott, N.F., Davies, E.A.: Electronic Processes in Non-Crystalline Materials. Clarendon Press, Oxford (1979)
25. Tauc, J.: Amorphous and Liquid Semiconductors. In: Tauc, J. (ed.) Plenum Press, New York (1974)
26. Gautam, C., Yadav, A.K., Singh, A.K.: A review on infrared spectroscopy of borate glasses with effects of different additives. ISRN Ceram. **2012**, 1–17 (2012)
27. Omri, K., El Ghoul, J., Alyamani, A., Barthou, C., El Mir, L.: Luminescence properties of green emission of SiO2/Zn2SiO4: Mn nanocomposite prepared by sol–gel method. Physica E **53**, 48–54 (2013)
28. Dimitrov, V., Sakka, S.: Electronic oxide polarizability and optical basicity of simple oxides. J. Appl. Phys. **79**, 1736–1740 (1996)

29. El-Mallawany, R., Abdalla, M.D., Ahmed, I.A.: New tellurite glasses, optical properties. Mater. Chem. Phys. **109**, 291–296 (2008)
30. Moelwyn-Hughes, E.A.: Physical Chemistry. Pergamon, London (1961)
31. El-Mallawany, R.: Optical properties of tellurite glasses. J. App. Physics **72**, 1774–1777 (1992)
32. Rawson, H.: Properties and Applications of Glass. Elsevier, Amsterdam (1980)
33. Azlan, M.N., Halimah, M.K., Shafinas, S.Z., Daud, W.M.: Electronic polarizability of zinc borotellurite glass system containing erbium nanoparticles. Mater. Express **5**, 211–218 (2015)
34. Herzfeld, K.F.: On atomic properties which make an element a metal. Phys. Rev. **29**, 701–705 (1927)
35. Honma, T., Sato, R., Benino, Y., Komatsu, T., Dimitrov, V.: Electronic polarizability, optical basicity and XPS spectra of Sb2O3–B2O3 glasses. J. Non-Cryst. Solids **272**, 1–13 (2000)
36. Azlan, M.N., Halimah, M.K., Shafinas, S.Z., Daud, W.M.: Polarizability and optical basicity of Er^{3+} ions doped tellurite based glasses. Chalcogenide Lett. **11**, 319–335 (2014)
37. Dimitrov, V., Sakka, S.: Linear and nonlinear optical properties of simple oxides. II. J. Appl. Phys. **79**, 1741–1745 (1996)
38. Wakkad, M.M., Shokr, EKh, Mohamed, S.H.: Optical and calorimetric studies of Ge–Sb–Se glasses. J. Non-Cryst. Solids **265**, 157–166 (2000)
39. Zhang, W.S., Zheng, J.G., Brück, E., Si, P.Z., Geng, D.Y., Zhang, Z.D.: Structure and magnetic properties of boron-oxide and boron-nitride coated iron nanocapsules. J. Mater. Sci. Technol. **26**(11), 1051–1056 (2010)
40. Kaewkhao, J., Siriprom, W., Insiripong, S., Ratana, T., Ratana, T., Kedkaew, C., Limsuwan, P.: Structural and magnetic properties of glass doped with iron oxide. J. Phys: Conf. Ser. **266**, 012012 (2011)
41. Cockayne, E., Li, L.: First-principles studies of the atomic, electronic, and magnetic structure of α-MnO2 (cryptomelane). Chem. Phys. Lett. **544**, 53–58 (2012)
42. Chen, W., Chen, C., Guo, L.: Magnetization reversal of two-dimensional superlattices of Mn_3O_4 nanocubes and their collective dipolar interaction effects. J. Appl. Phys. **108**, 043912–043912-8 (2010)
43. Crespo, Y., Seriani, N.: Electronic and magnetic properties of α-MnO_2 from abinitio calculations. Phys. Rev. B **88**, 144428–1444287 (2013)
44. Obaid, S.S., Sayyed, M.I., Gaikwad, D.K., Pawar, P.P.: Attenuation coefficients and exposure buildup factor of some rocks for gamma ray shielding applications. Radiat. Phys. Chem. **148**, 86–94 (2018)
45. Agar, O., Tekin, H.O., Sayyed, M.I., Korkmaz, M.E., Culfa, O.: Can Ertugay. Experimental investigation of photon attenuation behaviors for concretes including natural perlite. Results Phys. **12**, 237–243 (2019)
46. Rammah, Y.S., Sayyed, M.I., Abohaswa, A.S., Tekin, H.O.: electronic polarizability and shielding parameters of B_2O_3 glasses doped with SnO_2. Appl. Phys. A **124**, 560 (2018)
47. Murat, Kurudirek: Heavy metal borate glasses: potential use for radiation shielding. J. Alloy. Compd. **727**, 1227–1236 (2017)
48. Kurudirek, M., Chutithanapanon, N., Laopaiboon, R., Yenchai, C., Bootjomchai, C.: Effect of Bi_2O_3 on gamma ray shielding and structural properties of borosilicate glasses recycled from high pressure sodium lamp glass. J. Alloy. Compd. **745**, 355–364 (2018)
49. Sayyed, M.I., Ersundu, Ç.A.E., Ersundu, G., Kostka, P.L.: Investigation of radiation shielding properties for MeO–$PbCl_2$ –TeO_2 (MeO = Bi_2O_3, MoO_3, Sb_2O_3, WO_3, ZnO) glasses. Radiat. Phys. Chem. **144**, 419–425 (2018)
50. El-Mallawany, R., Sayyed, M.I., Dong, M.G., Rammah, Y.S.: Simulation of radiation shielding properties of glasses contain PbO. Radiat. Phys. Chem. **151**, 239–252 (2018)
51. Sayyed, M.I., Al Zaatreh, M.Y., Dong, M.G., Zaid, M.H.M., Matori, K.A., Tekin, H.O.: A comprehensive study of the energy absorption and exposure buildup factors of different bricks for gamma rays shielding. Res. Phys. **7**, 2528–2533 (2017)
52. Pawar, P.P., Bichile, K.G.: Studies on mass attenuation coefficient, effective atomic number and electron density of some amino acids in the energy range 0.122–1.330 MeV. Radiat. Phys. Chem. **92**, 22–27 (2013)
53. El-Mallawany, R., Sayyed, M.I., Dong, M.G.: Comparative shielding properties of some tellurite glasses: Part 2. J. Non-Cryst. Solids **474**, 16–23 (2017)
54. El-Mallawany, R., Abd El-Moneim, A.: Comparison between the elastic moduli of tellurite and phosphate glasses. Physica Status Solidi (A) Appl. Res. **166**, 829–834 (1998)
55. El-Mallawany, R.: Specific heat capacity of semiconducting glasses: Binary vanadium tellurite. Physica Status Solidi (A) Appl. Res. **177**, 439–444 (2000)